Acoustic Levitation assisted Contactless Printing of Microdroplets for Biomedical Applications

Tengteng Tang
Department of Aerospace and Mechanical Engineering,
School for Engineering of Matter, Transport and Energy
Arizona State University, Tempe, AZ 85281
ttang32@asu.edu
ASME Membership ID: 000103782844

Dylan Joralmon
Department of Aerospace and Mechanical Engineering,
School for Engineering of Matter, Transport and Energy
Arizona State University, Tempe, AZ 85281
dylan.joralmon@asu.edu

Tochukwu Anyigbo
Department of Materials Science and Engineering,
School for Engineering of Matter, Transport and Energy
Arizona State University, Tempe, AZ 85281
tanyigbo@asu.edu

Xiangjia Li[1]
Department of Aerospace and Mechanical Engineering,
School for Engineering of Matter, Transport and Energy
Arizona State University, Tempe, AZ 85281
xiangjia.li@asu.edu
ASME Membership ID: 000102217951

ABSTRACT

The cell is a microcapsule system wherein biological materials are encapsulated by a thin membrane, which provides valuable information on the metabolism, morphology, development, and signal transduction pathways of the studied cell. The cell inspired microdroplet has the characteristics of efficient nanoscale substance transportation, self-organization, and morphological adaptation. However, it is extremely difficult to manufacture such systems. Mostly vesicles such as liposomes, polymersomes, and microcapsules are first

[1] Corresponding author: xiangjia.li@asu.edu

produced by a high-pressure homogenizer and microfluidizer as an emulsion and then encapsulated microcapsules by the drop or emulsion method. Currently, acoustic levitation opens entirely new possibilities for creating bioinspired microdroplets because of its ability to suspend tiny droplets in an anti-gravity and non-contact manner. Herein, we propose contactless printing of single-core or multi-core cells inspired microdroplets via acoustic levitation. First, the oscillation mode and microscopic morphology of the droplets under different ultrasonic vibration frequencies are shown by simulation, and the curing characteristics of the shell structure under different ultraviolet illumination conditions are quantitatively measured. The feasibility of manufacturing multi-core microdroplets and manufacturing sub-millimeter-scale particles based on oil trapping is extensively studied. To explore the morphological adaptability of microdroplets, ferromagnetic Fe_3O_4 nanoparticles are used to give cells magnetic responsive properties and the microscopic deformation and motion in microfluidic channels under the magnetic field are characterized. Finally, the proposed printing method proves the versatility of in-space contactless printing of complex 3D beam structures and provides a powerful platform for developing biomedical devices and microrobots, and studying morphogenesis and synthetic biological systems.

Keywords: Contactless printing, acoustic levitation, microdroplets printing, photopolymerization, biomedical applications

1. INTRODUCTION

The bioinspired microdroplets have emerged as a promising avenue to gain deeper insights into the intricate structure and functions of biological cells. The fabrication of such synthetic entities has recently garnered substantial attention as a burgeoning field of research. Efforts to develop bioinspired microdroplets allow the investigation of autonomous systems with cell-like attributes in controlled conditions. Cells are highly intricate structures and have functional units called intracellular compartments, which regulate chemical and biological processes. This intracellular region is protected by a membrane that separates internal content from the surrounding. When developing

microdroplets that have cell-like functions, replicating the structure of the intracellular compartment is important to better mimic biological cell functionality. The bioinspired microdroplets exhibit diverse prospective applications, such as employment in the treatment of hepatic ailments, where current methods like transplants and cell therapies suffer challenges of negative immune response and limited efficiency duration [1]. Intriguingly, acoustic levitation is a counterintuitive phenomenon that capitalizes on the acoustic potential energies carried by sound waves to exert radiation force on small and lightweight objects. The resulting force levitates the object in an anti-gravity and contactless manner, directly opposing gravity. This phenomenon finds potential applications in constructing spherical microdroplets, as droplets suspended through acoustic levitation are well-suited for this purpose [2-10].

Currently, multiple recognized techniques exist for the production of bioinspired microdroplets. The two primary approaches in the fabrication of bioinspired microdroplets are the top-down and the bottom-up approaches [11, 12]. The top-down approach deals with generating a minimal cell from an already existing biological organism by removing cellular parts that are not essential to the survival of the organism and adding components for specific functions. However, the top-down approach often leaves genomes with unknown functions, thereby limiting the understanding of the minimal requirements for the survival of living cells. Correspondingly, the bottom-up approach is an additive approach that involves fabricating bioinspired microdroplets using basic units derived from natural organisms or synthetic processes [13-15]. This approach is often employed to construct structures by enclosing lipid-bounded aqueous droplets and

biomolecule complexes within a host droplet, with each compartment of the host droplet potentially containing different biochemical species. [16]. Some studies have demonstrated the utilization of organelle-like components that are analogous to the intracellular compartments and act as functional units, regulating sequential reactions and harvesting energy within the microdroplets [16]. However, the fabrication of bioinspired microdroplets poses challenges such as creating controlled distributions of biochemical reagents in multicompartmental structures and developing a low-cost, efficient method of acoustic printing of soft materials to mimic cell functionality.

The intricate intracellular compartments of cells pose a challenge for the fabrication of bioinspired microdroplets. Therefore, it is advantageous to investigate and establish compartmentalized structures that mimic those found in biological cells, which further serve as the foundation for the functionality of the cell. The ideal cellular structure consists of a hollow shell with an internal functional unit that is enclosed by a membrane, responsible for regulating vital processes. It is important to note that the architecture of the compartments is crucial in determining the functionality of the bioinspired microdroplets. Insufficient investigation has been conducted on the methods of compartmentalization in bioinspired microdroplets and the resulting functionality of these structures. This is partly due to the difficulty of producing multi-compartmental structures with controlled distributions of biochemical reagents, which involves a high-order emulsification process [16]. In comparison to other physical fields such as magnetic and electrical fields, acoustic-assisted additive manufacturing presents diverse potential applications. The contactless and interface-free nature of acoustic field manipulation

enables the trapping of small particles in standing waves and potential wells of the sound field [17]. However, the use of acoustic levitation by ultrasonic arrays has not been fully investigated and much of its applications in regard to fluid mechanics are still unknown [3]. Hence, there is a need to explore a low-cost and effective approach for acoustic printing of soft materials, which employs intracellular architecture to mimic the functions of cells [18-20]. Such an investigation has the potential to enhance drug delivery mechanisms and facilitate the production of high-quality microdroplets [21].

Here, we proposed a novel printing approach named acoustic levitation-assisted contactless droplet printing (ALCDP) for the fabrication of bioinspired microdroplets. The novelty of this method is reflected in the fact that the 3D printed complex structure is a multi-layer structure in the radial direction of the sphere, which is different from the traditional 3D printing that builds complex structures along a certain direction or plane [14, 22]. Firstly, the mechanism of ultrasonic levitation was revealed, and the sound pressure field map, droplet resonance morphology, and convection mode were visually displayed through simulation. Considering the light sensitivity of the materials and aiming to fabricate flexible and resilient shell structures under the guidance of the studied relationship between exposure time and curing thickness, the top-bottom-side (TBS), top-bottom (TB), and TBS+TB illumination strategies were developed for non-sensitive, sensitive, and semi-sensitive materials, respectively. Cured shell structures can be as thin as tens of microns and return to their original shape after being subjected to large ratios of deformation. Moreover, the oil trapping method provided an effective platform for the fabrication of single-core and multi-core cell structures, and its solidified spherical

structure can be as small as 300-800 µm, which is at least 3 times smaller than that of the direct injection method. Finally, we demonstrated the directional movement of the printed magnetic cell structure in the complex channel under the magnetic attraction and tracked the autonomous motion trajectory of the magnetic cell structure on the liquid surface under the influence of the magnetic field. Benefiting from ALCDP, printed microdroplets have the potential to enhance the understanding of biological cells and be used in drug delivery and treatment of chronic illnesses. We believe that the reported research is a step toward bioinspired microdroplets development in a contactless, autonomous, low-cost, and efficient way.

2. MATERIALS AND METHODS

2.1 Materials

Poly(ethylene glycol) diacrylate (Mn 700) (PEGDA), iron oxide, Irgacure 819 photoinitiator, and red oil dye were purchased from Sigma-Aldrich. The acoustic levitation set-up was purchased from Aliexpress. Oil, fluorescent dyes, water-based dyes were purchased from Tool Experts. Flexible 80A resin was purchased from Formlabs. Standard translucent photopolymer resin was purchased from Elegoo.

2.2 Material preparation

Three different photocuring strategies are designed for non-sensitive, sensitive and semi-sensitive materials respectively. 5 wt% iron oxide and 1 wt% Irgacure 819 photoinitiator were added to PEGDA and then vortex mixing for 5 minutes to obtain non-sensitive materials under TBS illumination strategy. Flexible 80A purchased from Formlabs used as a sensitive material under TB illumination strategy. The semi-sensitive

material under the TBS+TB illumination strategy was obtained by vortex mixing of Flexible 80A and 0.1 wt% red oil dye for 5 minutes. The material for making the magnetic core with high magnetic sensitivity was obtained by adding 10 wt% iron oxide and 1 wt% Irgacure 819 photoinitiator to PEGDA and vortex mixing for 5 minutes. The transparent photocurable PEGDA used to encapsulate the magnetic core was obtained by mixing PEGDA with 1 wt% Irgacure 819 photoinitiator vortex for 5 minutes. All vortex mixing materials were vacuumed to remove bubbles before ultrasonic levitation. Other materials appearing herein are used as received.

2.3 Droplet levitation and process planning

A commercially available TinyLev device [2] was used to ultrasonically suspend the droplet, which mainly consists of ultrasonic transducers, an Arduino nano controller, an L298N dual motor drive, 9 V DC power adaptor. Two pairs of transducers with a diameter of 10mm are fixed on a 3D-printed TinyLev frame, and transducers are arranged in three concentric circles on a hemispherical sphere. Transducers vibrate at a frequency of 40 kHz under the action of a high-frequency electrical signal applied by the driver, and then two sets of opposite hemispherical transducer arrays form standing waves in space, which are the positions corresponding to the droplets that can be suspended. The UV led with wattage of 1 W, voltage of 3 V, light intensity of 110 lm was purchased from Shenzhen Chanzon Technology Co., Ltd, which is used to initiate photopolymerization.

In terms of experimental operation, the droplet is manually extruded from the needle and hangs on the top of the needle under the constraints of surface tension, and then the droplet is slowly moved into the standing wave point (low-pressure area, as shown in the

bright yellow region of Fig.1a) of the ultrasonic field. Here, the 5 mL disposable syringes were purchased from BH SUPPLIES and the 30Ga blunt tip needles were purchased from CML Supply. The low-pressure area is first marked by the suspended foam, and then the liquid droplets are levitated in the low-pressure area near the coaxial line of the device. The volume of the droplet is determined spontaneously by its difficulty of separation from the needle and gravity, too little droplet is difficult to separate and too much will drip. After slowly removing the needle, the droplet is trapped in the low-pressure area and the contact surface between it and the needle is necked and fractured. Finally, it is stably suspended in the air. In the fabrication of a single-core cell structure, the base droplet is first suspended in the air, and then a hemispherical dye or magnetic solution at the tip of the needle is inserted into the base droplet. The second solution is trapped inside the base droplet after the needle is removed. A multi-core cell structure can be obtained by repeating this step.

2.4 Simulation of droplet oscillation mode

The simulations of the acoustic field and droplet oscillation morphology are conducted via COMSOL Multiphysics 5.6. Pressure Acoustics, Frequency Domain interface and Particle Tracing for Fluid Flow Interfaces are used to simulate the acoustic field and droplet oscillation morphology, respectively. A two-dimensional region is selected with the upper and lower ends of a circular curve and the left and right edges of a vertical line. The boundary of the curve is divided into odd parts and each segment is given the characteristics of high-frequency vibration at intervals to simulate the transducer's characteristics. The other boundaries are set as sound hard boundaries, and the material

inside the area is set as air. After calculation, the spatial distribution map of the ultrasonic field is obtained (Fig. 1a), and the sound pressure distribution is determined by [17]:

$$\begin{cases} \nabla \cdot \left(-\frac{1}{\rho_{\mathrm{c}}} \left(\nabla p_{\mathrm{t}} - \mathrm{q_d} \right) \right) - \frac{k_{\mathrm{eq}}^2 p_{\mathrm{t}}}{\rho_{\mathrm{c}}} = Q_{\mathrm{m}} \\ \mathrm{p_t} = p + p_{\mathrm{b}} \\ \mathrm{k_{eq}^2} = \left(\frac{\omega}{c_{\mathrm{c}}} \right)^2 - k_z^2 \end{cases} \tag{1}$$

where ρ_{c} is the quiescent density, p_{t} is the total pressure, $\mathrm{q_d}$ is the dipole domain source, k_{eq} is the wave number, Q_{m} is the monopole domain source, p_{b} is the background pressure, ω is the angular frequency, c_{c} is the speed of sound, and k_z is the out-of-plane wave number.

The droplets (or particles) are subjected to acoustophoretic radiation force, gravity force, and drag force in the acoustic field and remain suspended in the air in equilibrium. When the low-frequency modulation wave is superimposed on the ultrasonic wave with a frequency of 40 kHz, the acoustophoretic radiation force fluctuates periodically and the force balance of the droplet is broken, and oscillation occurs. The shape of the droplet changes from an ellipsoid to a complex pattern with varying numbers of nodes. The force F and vibration state of the droplet are respectively determined by the following three parts [23]:

$$\mathrm{F} = \mathrm{F_{rad}} + \mathrm{F}_g + \mathrm{F_D} = \frac{\mathrm{d}(m_{\mathrm{p}} \mathrm{v})}{\mathrm{d}t} \tag{2}$$

where $\mathrm{F_{rad}}$ is the acoustophoretic radiation force, F_g is the gravity force, $\mathrm{F_D}$ is the drag force, m_{p} is the particle mass, and v is the particle velocity. Accordingly,

$$\begin{cases} \mathrm{F}_{\mathrm{rad}} = V_p \left[f_1 \dfrac{1}{2\rho c^2} \langle p^2 \rangle - f_2 \dfrac{3}{4} \rho \langle v^2 \rangle \right] \\ f_1 = 1 - \dfrac{K_0}{K_p}, \quad f_2 = \dfrac{2(\rho_p - \rho)}{2\rho_p + \rho} \end{cases} \tag{3}$$

where V_p is the particle's volume, f_1, f_2 are the monopole and dipole scattering coefficients, respectively, ρ is the air density, c is the sound speed, p is the acoustic pressure, v is the acoustic velocity, K_0, K_p are the bulk moduli, and ρ_p is the particle density.

$$\mathrm{F}_g = m_p \mathrm{g} \frac{\rho_p - \rho}{\rho_p} \tag{4}$$

Where m_p is the particle mass, g is the gravitational acceleration, ρ is the air density, and ρ_p is the particle density.

$$\begin{cases} \mathrm{F}_\mathrm{D} = \dfrac{1}{\tau_p} m_p (\mathrm{u} - \mathrm{v}) \\ \tau_p = \dfrac{\rho_p d_p^2}{18\mu} \end{cases} \tag{5}$$

where τ is the diffusion coefficient, u is the acoustic velocity, v is the particle velocity, ρ_p is the particle density, d_p is the particle diameter, and μ is the air dynamic viscosity.

2.5 Magnetically driven motion and tracking

To test the motion of magnetic particles in the magnetic field, a microfluidic channel made of standard translucent photopolymer resin shaped (the ASU logo) was printed. The center-offset magnetic cells are first suspended on the liquid surface inside the channel, and then change the position of the magnet around the channel to drive the magnetic cells to move along the channel. Similarly, the magnetic cells are suspended in water filled the glass tank. When a magnet is close to the tank, the magnetic cells move to the edge of the tank under the action of magnetic force. A process of directional movement of

magnetic cells is recorded to track the motion. The video is converted into a series of single-frame pictures at different time slots after being imported into ImageJ. The pictures then need to be converted into grayscale images before using the Manual Tracking function. By selecting the target particles one by one, the particle positions at all times can be labeled, and finally, the movement trajectories of the particles can be obtained by overlaying these points to the last frame.

3. RESULTS AND DISCUSSION

3.1 Acoustic levitation assisted contactless droplet printing

As shown in Fig.1a, the transducers are placed on two horizontally opposed hemispherical frames, and ultrasonic waves generate high-pressure and low-pressure regions in the space as shown in the simulation of the acoustic field map, where the particles are suspended in the low-pressure regions. The node position of the standing wave is represented through the fluorescent droplets. Two different fluorescent dyes are vertically arranged in the air, emitting blue and red light when excited by UV incident light (Fig.1b). Controllable suspension of droplets and irradiation of UV light are necessary to levitate and cure photosensitive resins. By adjusting the exposure time and the components of the photosensitive mixture, fully cured droplets or spherical shell structures with different thicknesses can be obtained. Compared with pure PEGDA with 1 wt% Irgacure 819 photoinitiator, the curing characteristics of PEGDA mixed with 5 wt% iron oxide and 1 wt% Irgacure 819 photoinitiator indicates its low light penetration depth. Hence, it can be cured to form a thin shell structure, which has large deformation characteristics and can be completely flattened and restore the original shape for many

times (as shown in Fig.1c). In addition, we found that when the droplet is directly extruded and suspended with a syringe, it could be trapped at the node only when the volume of the droplet increased to a certain extent (1.5-3 mm in diameter) due to the restraint of surface tension as the droplet separate from the needle.

The oil droplet encapsulation method proposed in this paper can effectively reduce the size of photosensitive resin droplets (300-800 μm, Fig.1d), which provides the possibility for subsequent encapsulation of multilayer structures. At the same time, the solidified droplet cells containing the magnetic cores can achieve intricate motions driven by the magnetic force. For example, the movement in the ASU channel, balance under the action of various force fields, and the magnetic actuation and autonomous reset shown in Fig.1e. The magnetic nucleus cell structure in Fig.1e floats on the liquid surface against gravity under the action of the surface tension and buoyancy of the liquid. When the magnet approaches, the magnetic nucleus cells move away from the lower central area of the liquid level to the higher liquid level under the action of the magnetic force. After removing the magnet, the magnetic nucleus cells automatically return to the central area, and the corresponding driving trajectory can be obtained by repeating this cycle. Inspired by the concept of bioinspired microdroplet, transparent PEGDA was used to encapsulate the magnetic cores to obtain multilayer structures with outer shells and inner cores after fabricating smaller magnetic cores, such as the core-centered and biased cell structure in Fig.1f. Specifically, the magnetic droplet was first extruded to solidify as the inner core, and then the PEGDA solution was extruded to coat the inner core. As the droplet was rotated in the acoustic field, the inner core was biased to the edge under the

action of centrifugal force (as shown in the right image of 1f). Since the PEGDA700 has lower viscosity (130 cP), it is still possible for the core to be placed in the core of the structure (as shown in the left image of 1f), while the core cannot be centered at all when using 80A (1260 cP) to coat the core due to its high viscosity and poor fluidity.

3.2 Theoretic model and simulation of droplet under acoustic field

The droplet is suspended in the air by a 40 kHz ultrasonic wave and keeps the shape of an ellipsoid. When the modulation wave is superimposed on the ultrasonic wave, the intensity of the sound field will fluctuate, which causes the droplet to shake and deform. The shapes with different nodes can be obtained by controlling the frequency of the modulation wave. As shown in the simulation results in Fig.2, the droplet has three sharp corners (3 nodes) at 10 Hz, and the node of the droplet gradually increases with the increase of the modulation wave frequency. For example, the droplet has 8 nodes at 890 Hz. The diameter R and resonance frequency f_R of the droplet under the modulation wave are determined by the Rayleigh equation [9, 24]:

$$f_R = \frac{1}{2\pi}\sqrt{\frac{\sigma}{\rho R^3} l(l-1)(l+2)} \tag{6}$$

where σ is the surface tension, ρ is the density of the droplet, R is the droplet diameter, and l is the oscillation mode.

Theoretically, the higher the resonant frequency, the smaller the diameter under the same oscillation mode. The larger the oscillation mode value, the larger the diameter at the same resonant frequency. The effect of modulation wave on the suspended droplet is not only the change of shape, but also the convection inside the droplet. The larger the

deformation scale of the droplet, the faster the corresponding internal convection velocity. For example, the convection velocity at 230 Hz is several meters or tens of meters per second, while the deformation of the 890 Hz droplet is much smaller, and the internal convection is extremely slow. Therefore, convection inside the droplet can be manipulated through control of the resonant frequency, which provides an efficient platform for mixing materials at the microscale.

3.3 Investigation of photocuring strategy

Using photocurable materials, droplets can not only levitate under the sound field, but also solidify with controlled exposure time to obtain specific structures. Combined with magnetic materials, a drivable cell-like structure is fabricated with the ability to move directionally within complex channels. For light-sensitive materials, the curing characteristics are homogeneous, and the curing depth is logarithmically proportional to the input energy. The relationship between the curing depth of PEGDA solution and energy input is given by the Beer-Lamber's equations [25]:

$$C_d = d_p \ln\left(\frac{E_{\max}}{E_c}\right) \tag{7}$$

where d_p is the penetration depth of light into a photocurable PEGDA solution after a reduction in irradiation of *1/e* ; E_{max} is the peak energy of light illuminating on the photocurable PEGDA solution; and E_c is the minimum energy for the photocurable PEGDA solution to be solidified.

The curing property of the PEGDA and iron oxide mixture are not as sensitive as the pure photocurable PEGDA. The curing depth decreased due to the light-shielding

properties of the iron oxide particles. The curing property of the mixture can be determined by Griffith and Halloran's equation [26, 27]:

$$C_d = \left(\frac{\eta}{\eta_P - \eta}\right)\frac{\lambda^2}{a}\ln\left(\frac{t}{t_c}\right)\frac{1}{\varphi} \tag{8}$$

where η and η_P are the refractive indexes of the PEGDA and iron oxide particle, respectively, λ is the wavelength of incident light, a is diameter of the iron oxide particles, t and t_c is the exposure time and critical exposure time respectively, and φ is the concentration of iron oxide particles.

Intrinsically, droplet suspensions are suitable for the fabrication of spheres, disks and shell structures. When the droplet is fully solidified, the shape of the solid is determined by the droplet's volume and surface tension. The smaller the droplet, the closer the solidified entity is to a sphere. On the contrary, the droplet is in a disc structure under the compression of the sound field and the action of centrifugal force. If the volume of the liquid continues to increase, the surface of the droplet ruptures, and the droplet is unbalanced and splashes around under the action of centrifugal force and acoustophoretic radiation force. Fig.3a shows the process of solidifying the shell in this study. First, the PEGDA droplets containing the photoinitiator are extruded and gathered at the tip of the needle under the action of surface tension, and then the tip of the needle is placed in a low-pressure sound field. When the needle is removed from the acoustic field, the droplet is trapped in the low-pressure area. Once the droplet volume is sufficient, the contact surface between the droplet and the needle is necked and broken, and finally suspends in the nodes. If the volume of the droplet is too small, it escapes from

the low-pressure area under the pulling of the needle and cannot achieve independent suspension. The photocuring process is then initiated by controlling the UV light sources (Fig.1a) on the top, bottom and sides of the device. The irradiation time is also precisely controlled to avoid the droplets being completely solidified or the top and bottom of the droplets not being cured due to insufficient light intensity. The cross-sectional view of the sample in Fig. 3a clearly demonstrates the feasibility of fabricating shells by combining ultrasonic suspension droplets and photocuring. We then further study the curing characteristics and corresponding curing strategies of different materials.

The material in Fig.3b is PEGDA with 5 wt% iron oxide and 1 wt% Irgacure 819 photoinitiator. The large amount of iron oxide absorbs the incident light and reduces the penetration depth of light, which helps solidify the shell structure without fully solidifying as easily as pure PEGDA. In this regard, the TBS illumination strategy is used to fabricate the shell structure. The stronger UV light on the side cures the side of the droplet but is not enough to cure the top and bottom of the droplet, so the weaker light source at the top and bottom aids in solidifying the upper and lower areas of the droplet (Fig.3b-1). Finally, a shell structure with droplets inside as shown in Fig.3b-2 is obtained, and the sides of the shell are significantly thicker than the upper and lower regions as shown in the cross-sectional view in Fig.3b-3. By measuring the mean value of the shell thickness, the relationship between the thickness and the illumination time in Fig.3b-4 is obtained. Obviously, the shell thickness increases steadily from 45 μm at 10 s to 160 μm at 90 s with increasing illumination time. Subsequently, the shell thickness no longer increases significantly even with continued illumination because the incident light is absorbed by

the iron oxide and cannot penetrate deeper into the droplet. It is worth noting that when the illumination time is less than 10 s, the bottom and top regions of the droplet are not completely cured, and finally only a hollow ring structure or a semi-cured colloidal state can be formed.

For light-sensitive materials, light from the side causes the suspended droplets to solidify rapidly, making it difficult to fabricate thin shell structures. Therefore, a strategy of TB lighting is chosen when using the easily photocurable Flexible 80A material in Fig.3c. Since the material is transparent, the areas on the left and right edges of the droplets are also prone to curing (Fig.3c-1). Due to the excellent elasticity of the material, the thin shell structure containing the uncured liquid in Fig.3c-2 can recover its original shape without cracking and leaking even after being subjected to large-scale compressive deformation. The cross-sectional view of the thin shell structure in Fig.3c-3 exhibits good thickness uniformity. As shown in Fig.3c-4, the shell thickness gradually increased from 50 μm at 45 s to 130 μm at 75 s, and then if the illumination time continued to increase to 90 s, the thickness would sharply increase to a value of 360 μm, which is due to the complete solidification of the droplets. In addition, when the illumination time is less than 45 s, the energy input of UV light is not enough to solidify the droplets, and the droplets still maintain a colloidal state without a thin shell outer layer.

When the solidification characteristics of the liquid are between sensitive and semi-sensitive states, both the TBS and TB strategies described above are no longer applicable, where TBS makes the left and right edges of the droplet solidify too thick, and TB cannot effectively solidify the left and right edges. Therefore, through a proper combination of

TBS and TB irradiation time, the upper and lower regions of the droplet can be effectively cured while controlling the curing thickness of the left and right edges to avoid over-curing and under-curing (Fig.3d-1). We found that the droplet surface was completely solidified to form a thin shell structure (Fig.3d-2,3) when the TBS and TB times were 45 s and 180 s respectively as shown in Fig.3d-4, whose corresponding thickness was 100 μm. As a result, we propose illumination strategies for materials with different photocurable properties, which provide an effective means to precisely control shell thickness and enable more complex mono- and or multi-layer printing.

3.4 ALCDP fabricated microdroplets

After discussing suspending individual droplets and solidifying thin shell structures, the most obvious problems are the low structural complexity and the excessively large droplet size. Here, we propose the fabrication of single-core or multi-core structures based on oil trapping. The specific steps are to first suspend the oil droplets, then insert a needle containing a water-soluble dye into the oil droplet to inject the dye, and finally slowly withdraw the needle to ensure oil/dye droplet is still in the low-pressure region (Fig.4a). The dyes are phase-separated from the oil droplets under the coating of the hydrophilic group of the oil droplets and are not mutually miscible, and the two are independently and stably suspended in the air. Similarly, oil/dye structures with different color cores are obtained by replacing different dyes (Fig.4b). To further demonstrate the versatility of the oil trapping method, dyes with different colors were simultaneously injected into oil droplets to form multinucleated structures as shown in Fig.4c. Since the volume of oil droplets that can be suspended in the acoustic field is determined by the

power and frequency of ultrasound transducers, the injecting volume of dyes is limited when fabricating a multi-core structure (Fig.4b). The volume of different dyes added each time needs to be precisely controlled to achieve multi-core architecture. It can be found that when a single core or a double core is injected, the cores can still well maintain the spherical structure, and do not fuse with the help of the oil membrane coating. After adding to three cores, the inner core structure is deformed due to the limited space inside the droplet, and the dye boundaries contact, squeeze and deform with each other. In the penta-core structure, the dyes are almost mixed, and the boundaries are completely fitted. But the oil membrane does not allow the exchange of different dyes and maintains a clear curved boundary.

In order to solve the defects of excessively large volume and flat shape of directly injected droplets, the photocurable material can be injected into the oil droplets to form nearly spherical droplets with the size of hundreds of microns. As shown in Fig.4d, the size of the spheres fabricated by oil trapping is 3 times smaller than that of the injected droplets, and the diameter can be reduced by an order of magnitude by controlling the droplet volume in the experiments. After successful solidification of the single-core droplet, a quad-core structure resembling the cleavage stage of cell division is fabricated (Fig.4e). Since the viscosity and surface tension of the black photosensitive material (PEGDA+10 wt% iron oxide) are higher than those of the dye, the boundary does not completely contact like the multi-dye cores even if there are four cores at the same time. Meanwhile, a liquid bridge is formed due to the micro-exchange of the materials between the adjacent inner cores after a long time of pressure at the contact point. The four cores

are not completely separated but interconnected as one after curing. The phenomenon of being independent of each other before solidification and becoming one after solidification provides an effective research method for biomimetic research on the material exchange between multinuclear structures.

After studying the photocuring properties of thin shell structures and proposing methods to fabricate multicore cell structures, different application scenarios are represented. When the droplet is suspended in the air, it not only vibrates in space, but also rotates at an irregular high speed along the longitudinal axis. To visualize the rotation of the droplet, two magnetic droplets are injected into the oil droplet, which rotates inside the droplet edge under the action of centrifugal force. Fig.5a shows the positions of the dumbbell-shaped structure composed of two cores at different time slots, and the corresponding rotation period lasts 0.4 s. Inspired by the viscous resistance existing at the liquid interface of different flow rates, the magnetic cores can be forced to park at the edge region of the droplet by magnets. At this time, the high-speed flowing droplet receives frictional resistance when flowing through the stationary magnetic core. After a period, the droplet stops spinning and the inner core remains stationary. When the magnet is removed, the inner core moves towards the center of the droplet. The droplet continues to rotate, and the inner core is also driven by the flow inside the oil droplet to rotate together. Next, a thin shell structure with a free-moving magnetic core inside is fabricated. The extruded micro-curable PEGDA droplet rests at the tip of the needle under the action of surface tension, which is suspended in the ultrasonic field along with the magnetic helical structure tethered inside the droplet. By precisely controlling the

exposure time of UV light, a cell-like structure with a solidified surface while the interior is still liquid and a magnetic core that can move freely is fabricated. As shown in Fig.5b, the helical magnetic core is driven by the magnet at different positions. To further demonstrate the ability of magnetically driven directional movement, a spherical structure with an offset magnetic core freely and smoothly traverses an ASU-shaped microfluidic channel under the applied magnetic field (Fig.5c). It can be seen that the smaller magnetic core part at the head always faces the front when moving, which is consistent with the direction of the force. The magnetically driven directional mobile particles demonstrated here can be applied to target drug delivery in complex human blood vessels because the magnetic field has good permeability, the particles themselves do not need to carry energy supply and the driving method is harmless to the human body. In addition, the magnetic cells suspended on the liquid surface reach a balance under the action of buoyancy, gravity, surface tension, and magnetic force (Fig.5d). When the magnet gradually approaches the glass tank, the increase of the strength of the magnetic field makes the magnetic cells overcome the gravity and surface tension, and gradually move from the central region to the edge. Experimental results have shown that the distance between the magnetic cell and the center of the glass tank is inversely related to the distance between the magnet and the magnetic cell.

4. CONCLUSION

In this work, a contactless suspension of droplets to fabricate mononuclear or multinucleated bioinspired microdroplet structures was proposed. The mechanism of acoustic levitation and the simulations of the acoustic field, droplet morphology and

internal convection were elaborated and demonstrated. In order to fabricate the shell structure, the TBS illumination strategy for non-photosensitive materials, TB illumination strategy for sensitive materials, and TBS+TB illumination strategy for semi-sensitive materials were developed according to the light sensitivity of the materials. Correspondingly, the relationship between exposure time and curing thickness was investigated. Moreover, the oil trapping-based manufacturing process exhibits excellent properties for the fabrication of mononuclear or multinucleated cellular structures, which can solidify spheroid structures that are at least 3 times smaller than those cured with direct injection. Finally, we presented that the magnetic nuclei stop droplet spin, the ability of magnetic cell structures to move directionally within complex channels driven by the magnet, and the dynamic equilibrium of magnetic cell on the liquid surface under the buoyancy, gravity, surface tension, and magnetic force. Overall, the proposed research investigates the use of acoustic levitation and microfluidics to print multi-compartment microdroplets. This study presents a new approach to processes such as separation, mixing, and evaporation that occur in the generation of new smart materials and structures. The combination of droplet microfluidics and acoustic manipulation (which are contactless and non-invasive) can combat the challenge of high-order emulsification during the fabrication of microdroplets. This strategy also explores a new manufacturing tool for various applications that are of high value to the biomedical industry and in space printing. In the future, 1) the different solidification properties of the upper and lower and side regions of the droplet will be extensively studied, shell with uniform thickness can be made by homogenizing the light intensity; 2) Create microfluidic

channels to inject multi-nucleated droplets; 3) Build a multi-needle injection system to fabricate shell-liquid cavity-core structure. The droplet morphology, internal convection, irregular spin, and their potential in vitro or in vivo biological applications will be further explored. The possibility of using ultrasonic levitation to fabricate variable-focus liquid optical lenses will be systematically investigated [28].

ACKNOWLEDGEMENTS

The authors acknowledge ASU Startup Funding, ASU FSE Strategic Interest Seed Funding, and National Science Foundation (NSF grant No. CMMI-2114119).

NOMENCLATURE

ALCDP	Acoustic levitation assisted contactless droplet printing
PEGDA	Poly(ethylene glycol) diacrylate
TBS	top-bottom-side
TB	top-bottom
DC	direct current
ρ_c	quiescent density
p_t	total pressure
q_d	dipole domain source
k_{eq}	wave number
Q_m	monopole domain source
p_b	background pressure
ω	angular frequency
c_c	speed of sound
k_z	out-of-plane wave number
F	total force
F_{rad}	acoustophoretic radiation force
F_g	gravity force
F_D	drag force
m_p	particle mass
v	particle velocity
V_p	particle's volume

f_1	monopole scattering coefficient
f_2	dipole scattering coefficient
ρ	air density
c	sound speed
p	acoustic pressure
v	particle velocity
K_o	air bulk moduli
K_p	particle bulk moduli
ρ_p	particle density
g	gravitational acceleration
u	acoustic velocity
d_p	particle diameter
μ	air dynamic viscosity
f_R	resonance frequency
σ	surface tension
R	droplet diameter
l	oscillation mode
C_d	curing depth
d_p	light penetration depth
E_{max}	peak light intensity
E_c	photocuring energy threshold

η	refractive index of the photocurable PEGDA
η_P	refractive index of the iron oxide particle
λ	wavelength of incident light
a	diameter of the iron oxide particles
t	exposure time
t_c	critical exposure time
φ	concentration of magnetic iron oxide particles

503
504

REFERENCES

[1] Zou, D., Wang, H., Liu, X., Xu, Z. P., Roberts, M. S., and Zhao, C. X., "Artificial cells for the treatment of liver diseases," (1878-7568 (Electronic))

[2] Marzo, A., Barnes, A., and Drinkwater, B. W., 2017, "TinyLev: A multi-emitter single-axis acoustic levitator," Review of Scientific Instruments, 88(8), p. 085105. DOI: 10.1063/1.4989995

[3] Watanabe, A., Hasegawa, K., and Abe, Y., 2018, "Contactless Fluid Manipulation in Air: Droplet Coalescence and Active Mixing by Acoustic Levitation," Scientific Reports, 8(1), p. 10221. DOI: 10.1038/s41598-018-28451-5

[4] Polychronopoulos, S., and Memoli, G., 2020, "Acoustic levitation with optimized reflective metamaterials," Scientific Reports, 10(1), p. 4254. DOI: 10.1038/s41598-020-60978-4

[5] Hirayama, R., Christopoulos, G., Martinez Plasencia, D., and Subramanian, S., "High-speed acoustic holography with arbitrary scattering objects," Science Advances, 8(24), p. eabn7614. DOI: 10.1126/sciadv.abn7614

[6] Marzo, A., Seah, S. A., Drinkwater, B. W., Sahoo, D. R., Long, B., and Subramanian, S., 2015, "Holographic acoustic elements for manipulation of levitated objects," Nature Communications, 6(1), p. 8661. DOI: 10.1038/ncomms9661

[7] Ochiai, Y., Hoshi, T., and Rekimoto, J., 2014, "Three-Dimensional Mid-Air Acoustic Manipulation by Ultrasonic Phased Arrays," PLOS ONE, 9(5), p. e97590. DOI: 10.1371/journal.pone.0097590

[8] Morales, R., Ezcurdia, I., Irisarri, J., Andrade, M. A. B., and Marzo, A., 2021, "Generating Airborne Ultrasonic Amplitude Patterns Using an Open Hardware Phased Array," Applied Sciences.

[9] Foresti, D., Nabavi, M., Klingauf, M., Ferrari, A., and Poulikakos, D., 2013, "Acoustophoretic contactless transport and handling of matter in air," Proceedings of the National Academy of Sciences, 110(31), pp. 12549-12554. DOI: 10.1073/pnas.1301860110

[10] Chen, K., Wu, M., Guo, F., Li, P., Chan, C. Y., Mao, Z., Li, S., Ren, L., Zhang, R., and Huang, T. J., 2016, "Rapid formation of size-controllable multicellular spheroids via 3D acoustic tweezers," Lab on a Chip, 16(14), pp. 2636-2643. DOI: 10.1039/C6LC00444J

[11] Tanwar, L., and Devaraj, N. K., 2022, "Engineering materials for artificial cells," Current Opinion in Solid State and Materials Science, 26(4), p. 101004. DOI: 10.1016/j.cossms.2022.101004

[12] Chen, L., Xiao, Y., Wu, Q., Yan, X., Zhao, P., Ruan, J., Shan, J., Chen, D., Weitz, D. A., and Ye, F., 2021, "Emulsion Designer Using Microfluidic Three-Dimensional Droplet Printing in Droplet," Small, 17(39), p. 2102579. DOI: 10.1002/smll.202102579

[13] Tiwari, L., Tang, T., Rong, J., Shan, W., Yang, Y., and Li, X., 2022, "Thermoelectric Material Fabrication using Mask Image Projection Based Stereolithography Integrated with Hot Pressing," Journal of Material Science and Technology Research, 9(1), pp. 105-113. DOI: 10.31875/2410-4701.2022.09.11

[14] Tengteng, T., Dylan, J., and Xiangjia, L., 2023, "3D Printing of Biomimetic Functional Nanocomposites Via Vat Photopolymerization," Advances in 3D Printing, S. Ashutosh, ed., IntechOpen, Rijeka, p. Ch. 5. DOI: 10.5772/intechopen.110413

[15] Tang, T., Alfarhan, S., Jin, K., and Li, X., 2023, "4D Printing of Seed Capsule-Inspired Hygro-Responsive Structures via Liquid Crystal Templating-Assisted Vat Photopolymerization (Adv. Funct. Mater. 5/2023)," Advanced Functional Materials, 33(5), p. 2370029. DOI: 10.1002/adfm.202370029

[16] Li, J., Jamieson, W. D., Dimitriou, P., Xu, W., Rohde, P., Martinac, B., Baker, M., Drinkwater, B. W., Castell, O. K., and Barrow, D. A., 2022, "Building programmable multicompartment artificial cells incorporating remotely activated protein channels using microfluidics and acoustic levitation," Nature Communications, 13(1), p. 4125. DOI: 10.1038/s41467-022-31898-w

[17] Zang, D., Yu, Y., Chen, Z., Li, X., Wu, H., and Geng, X., 2017, "Acoustic levitation of liquid drops: Dynamics, manipulation and phase transitions," Advances in Colloid and Interface Science, 243, pp. 77-85. DOI: 10.1016/j.cis.2017.03.003

[18] Tang, T., Ahire, B., and Li, X., 2022, "Scalable Multi-Material Additive Manufacturing of Bioinspired Polymeric Material With Metallic Structures Via Electrically Assisted Stereolithography," Journal of Manufacturing Science and Engineering, 145(1). DOI: 10.1115/1.4055793

[19] Joralmon, D., Alfarhan, S., Kim, S., Tang, T., Jin, K., and Li, X., 2022, "Three-Dimensional Printing of Liquid Crystals with Thermal Sensing Capability via Multimaterial Vat Photopolymerization," ACS Applied Polymer Materials, 4(4), pp. 2951-2959. DOI: 10.1021/acsapm.2c00322

[20] Tang, T., Alfarhan, S., Jin, K., and Li, X., 2023, "4D Printing of Seed Capsule-Inspired Hygro-Responsive Structures via Liquid Crystal Templating-Assisted Vat Photopolymerization," Advanced Functional Materials, 33(5), p. 2211602. DOI: 10.1002/adfm.202211602

[21] Sakamoto, R., Izri, Z., Shimamoto, Y., Miyazaki, M., and Maeda, Y. T., 2022, "Geometric trade-off between contractile force and viscous drag determines the actomyosin-based motility of a cell-sized droplet," Proceedings of the National Academy of Sciences, 119(30), p. e2121147119. DOI: DOI:10.1073/pnas.2121147119

[22] Tang, T., Dwarampudi, G. S. K. A. R., and Li, X., 2023, "Electrically Assisted Vat Photopolymerization of Bioinspired Hierarchical Structures with Controllable Roughness for Hydrophobicity Enhancement Using Photocurable Resin/Carbon Nanotube," JOM, 75(7), pp. 2137-2148. DOI: 10.1007/s11837-023-05889-1

[23] Gor'kov, L. P., 1962, "On the Forces Acting on a Small Particle in an Acoustical Field in an Ideal Fluid," Soviet Physics Doklady, 6, p. 773

[24] Shen, C. L., Xie, W. J., and Wei, B., 2010, "Parametrically excited sectorial oscillation of liquid drops floating in ultrasound," Physical Review E, 81(4), p. 046305. DOI: 10.1103/PhysRevE.81.046305

[25] Jacobs, P. F., 1992, Rapid prototyping & manufacturing: fundamentals of stereolithography, Society of Manufacturing Engineers.

[26] Joyee, E. B., Lu, L., and Pan, Y., 2019, "Analysis of mechanical behavior of 3D printed heterogeneous particle-polymer composites," Composites Part B: Engineering, 173, p. 106840. DOI: 10.1016/j.compositesb.2019.05.051

[27] Yasui, M., and Ikuta, K., 2017, "Modeling and measurement of curing properties of photocurable polymer containing magnetic particles and microcapsules," Microsystems & Nanoengineering, 3(1), p. 17035. DOI: 10.1038/micronano.2017.35

[28] Zhu, Y., Tang, T., Zhao, S., Joralmon, D., Poit, Z., Ahire, B., Keshav, S., Raje, A. R., Blair, J., Zhang, Z., and Li, X., 2022, "Recent advancements and applications in 3D printing of functional optics," Additive Manufacturing, 52, p. 102682. DOI: 10.1016/j.addma.2022.102682

586 **Figure Captions List**
587

Fig. 1 Acoustic levitation assisted contactless droplet printing process and sample demonstration. (a) Illustration of ALCDP set-up and simulation of acoustic field distribution; (b) acoustic levitation fluorescent droplet array under UV light; (c) high deformation rate and recoverability of thin shell structure; (d) the solidified extruded core and oil trapped core are compared to the dimensions of a penny; (e) trajectory of a magnetically driven center-offset cell structure with magnetic core in water; (f) demonstration of center and center-offset magnetic cell structures and the fabrication results.

Fig. 2 Simulation of droplet oscillation morphology and electrical signal input of the ultrasonic suspension wave. (a-f) The droplet morphology and the number of nodes at different modulation wave frequencies.

Fig. 3 Ultrasonic levitation fabrication of thin shell structures and photocuring strategy. (a) Ultrasonic levitation and photocuring process of droplets; (b) TBS curing strategy and curing characteristics of non-sensitive materials; (c) TB curing strategy and curing characteristics of sensitive materials; (d) TBS/TB curing strategy and curing characteristics of semi-sensitive materials. The horizontal axes of Fig.3d-4 represent the illumination time of TBS and TB, respectively, and the thickness of the resulting cured shell.

Fig. 4 Oil trapping-based printing strategy. (a) The flow of dye core trapped in the suspended oil droplets; (b) oil droplets with mononuclear dye core; (c) the process of injecting different dye cores into oil droplets; (d) oil trapping-based fabrication of submillimeter-scale magneto-nucleated structure; (e) multiple magnetic nuclei trapped by oil droplets without fusion.

Fig. 5 Magnetic response of the ALCDP printed magnetic core structure. (a) The magnetic core prevents the droplet from rotating under the action of the magnetic field; (b) the motion of the submillimeter-scale helical structure wrapped by the shell under the magnetic field; (c) the directional movement of the magnetic core structure in the ASU channel under the magnetic drive; (d)The deviation of the magnetic core structure suspended at the liquid surface under different magnetic field strengths.

588
589
590

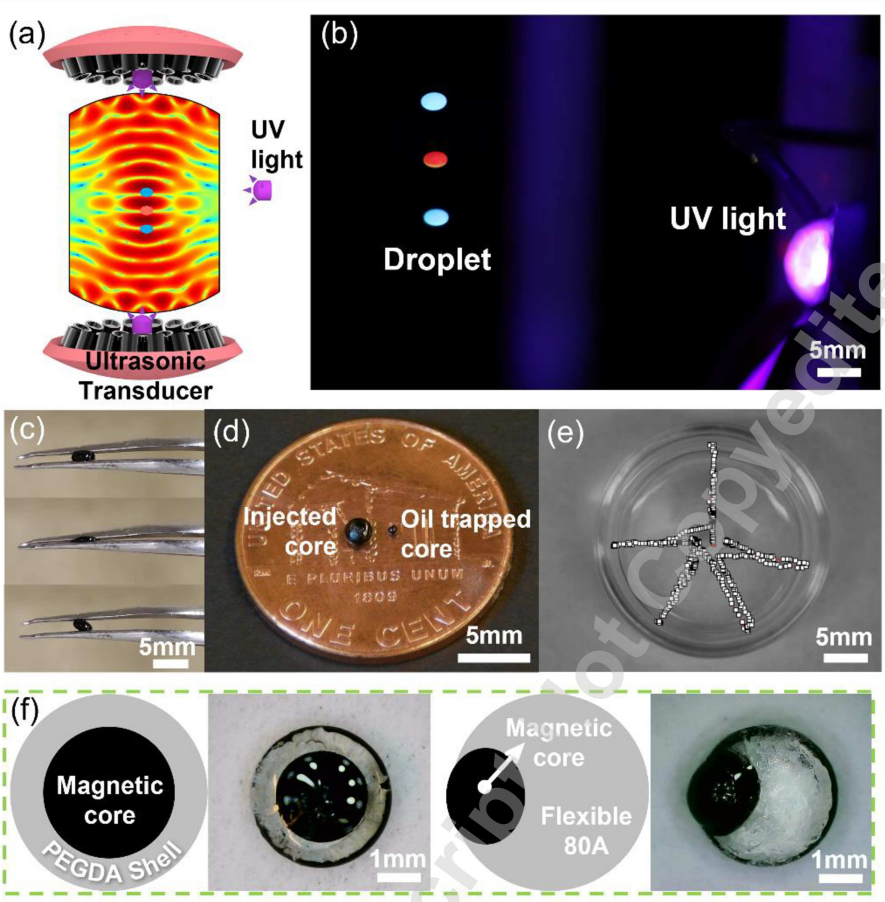

Fig. 1 Acoustic levitation assisted contactless droplet printing process and sample demonstration. (a) Illustration of ALCDP set-up and simulation of acoustic field distribution; (b) acoustic levitation fluorescent droplet array under UV light; (c) high deformation rate and recoverability of thin shell structure; (d) the solidified extruded core and oil trapped core are compared to the dimensions of a penny; (e) trajectory of a magnetically driven center-offset cell structure with magnetic core in water; (f) demonstration of center and center-offset magnetic cell structures and the fabrication results.

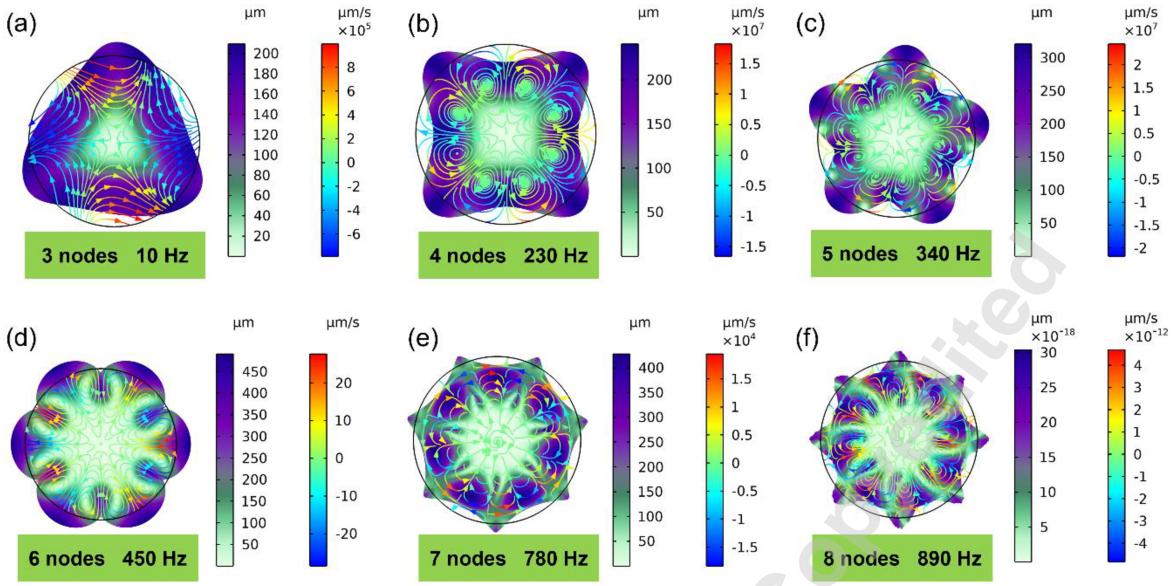

Fig. 2 Simulation of droplet oscillation morphology and electrical signal input of the ultrasonic suspension wave. (a-f) The droplet morphology and the number of nodes at different modulation wave frequencies.

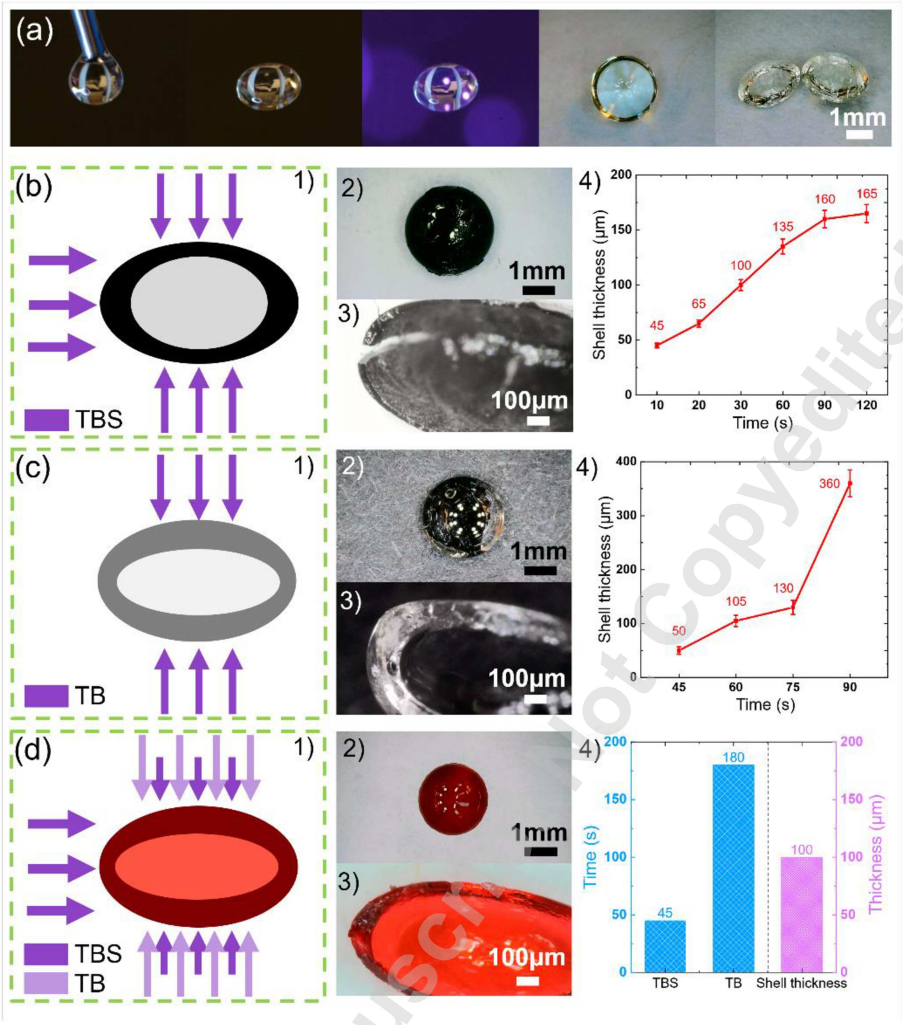

Fig. 3 Ultrasonic levitation fabrication of thin shell structures and photocuring strategy. (a) Ultrasonic levitation and photocuring process of droplets; (b) TBS curing strategy and curing characteristics of non-sensitive materials; (c) TB curing strategy and curing characteristics of sensitive materials; (d) TBS/TB curing strategy and curing characteristics of semi-sensitive materials. The horizontal axes of Fig.3d-4 represent the illumination time of TBS and TB, respectively, and the thickness of the resulting cured shell.

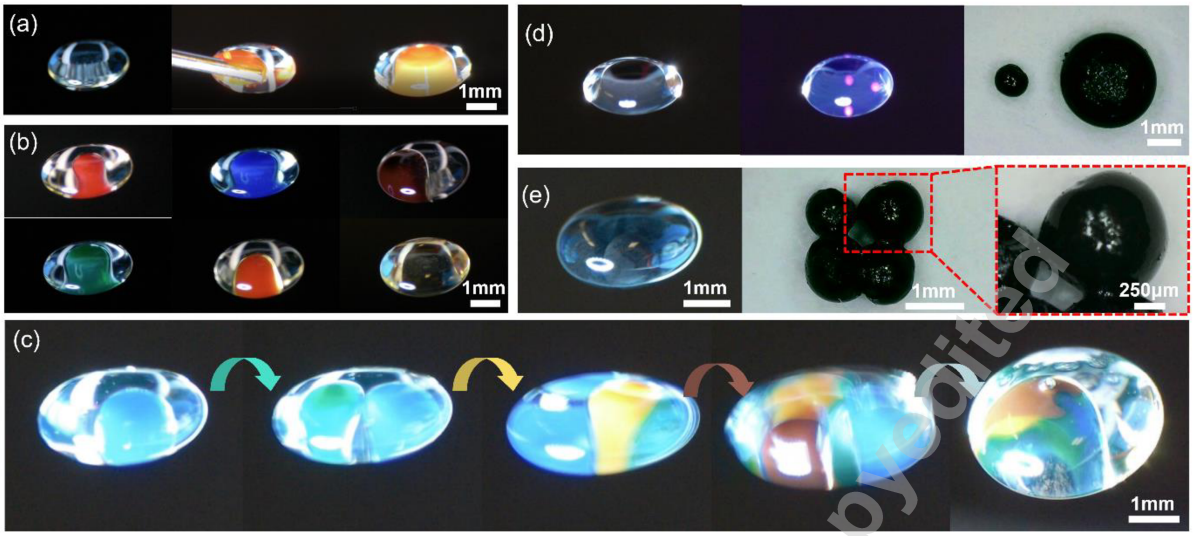

Fig. 4 Oil trapping-based printing strategy. (a) The flow of dye core trapped in the suspended oil droplets; (b) oil droplets with mononuclear dye core; (c) the process of injecting different dye cores into oil droplets; (d) oil trapping-based fabrication of submillimeter-scale magneto-nucleated structure; (e) multiple magnetic nuclei trapped by oil droplets without fusion.

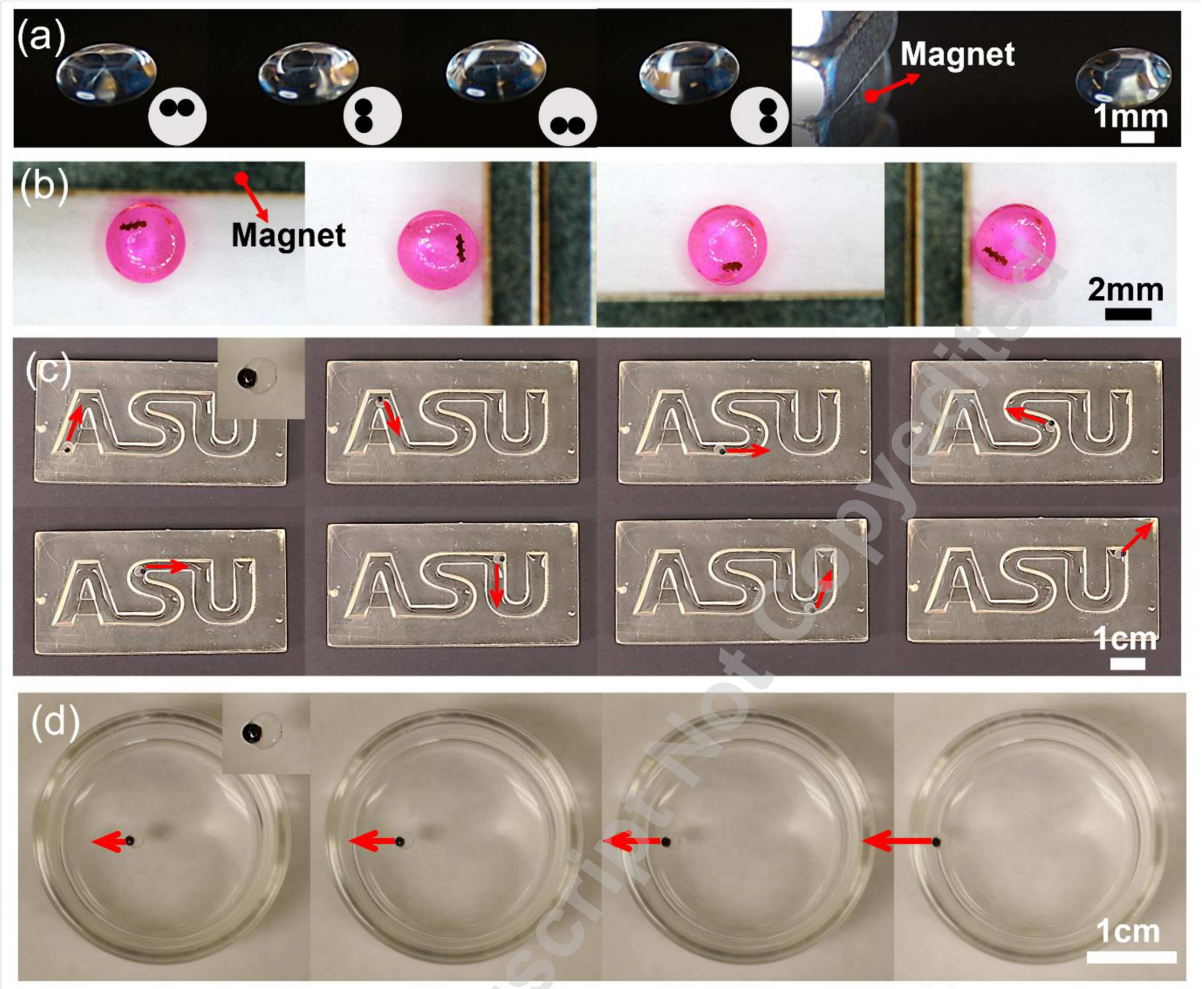

Fig. 5 Magnetic response of the ALCDP printed magnetic core structure. (a) The magnetic core prevents the droplet from rotating under the action of the magnetic field; (b) the motion of the submillimeter-scale helical structure wrapped by the shell under the magnetic field; (c) the directional movement of the magnetic core structure in the ASU channel under the magnetic drive; (d)The deviation of the magnetic core structure suspended at the liquid surface under different magnetic field strengths.